OSTEOGENSIS MIMICKING SCAFFOLDS FOR BOME TISSUE ENGINEERING

Nuttamon YOORONG[1], Jutakan THONGLAM[1], Varistha METWM[1], Sittichat CHUKAEW[3], Premikar SRIFA[2], Mattana KHANGKHAMANO[3], Jirut MEESANE[1]

1 Institute of Biomedical Engineering, Department of Biomedical Science and Biomedical Engineering, Faculty of Medicine, Prince of Songkla University, Thailand
2 Division of Biomedical Science, Department of Biomedical Science and Biomedical Engineering, Faculty of Medicine, Prince of Songkla University, Thailand
3 Department of Mining and Materials Engineering, Faculty of Engineering, Prince of Songkla University, Thailand; jirutmeesane999@yahoo.co.uk

ABSTRACT

Osteoarthritis (OA) is a degenerative joint disease characterized by cartilage degeneration and inflammation, which can affect various joints throughout the body. In severe cases, surgical intervention may be required, with tissue engineering scaffolds offering a potential approach for tissue replacement and regeneration. In this study, a biphasic scaffold consisting of a silk fibroin film affixed to a silk fibroin/magnesium chloride ($MgCl_2$) sponge was developed for potential application in osteoarthritis treatment. Previous studies have investigated silk fibroin film combined with collagen type I and polyvinyl alcohol (PVA). Therefore, this study aimed to mimic the functional extracellular matrix (ECM) using a silk fibroin film and a collagen type I/PVA/$MgCl_2$ scaffold to support bone tissue regeneration. The scaffold morphology was characterized using scanning electron microscopy (SEM). The biological functionality of the scaffolds was evaluated using bone cell culture, and cell proliferation was assessed to determine cellular responses to the scaffolds. In addition, Fourier-transform infrared (FT-IR) spectroscopy was used to characterize the chemical functional groups and molecular interactions within the scaffolds. The silk fibroin film and collagen type I/PVA/$MgCl_2$ scaffold demonstrated potential for improving scaffold performance, particularly in terms of cell adhesion and proliferation. These findings suggest that the developed scaffold has potential as a tissue engineering scaffold for bone tissue regeneration and may be applicable to the treatment of osteoarthritis.

Keywords: Osteoarthritis, scaffolds, Silk fibroin, collagen1, PVA, $MgCl_2$

CITATION INFORMATION: Yoorong, N., Thonglam, J., Metem, V., Chukaew, S., Srifa, P., Khangkhamano, M., & Meesane, J. (2026). osteogenesis mimicking scaffolds for bone tissue engineering. *Procedia of Multidisciplinary Research, 4(9), 89.*

INTRODUCTION

Bone is a highly specialized connective tissue that provides structural support, protects internal organs, and facilitates body movement. Beyond its mechanical functions, bone plays essential roles in several physiological processes, including hematopoiesis, maintenance of stem cell niches, and the regulation and storage of minerals such as calcium and phosphate (Arden, N., & Nevitt, M.C, 2006). Therefore, bone damage resulting from trauma, injury, infection, or degenerative disorders can significantly impair physical function and negatively affect overall quality of life. Among the various conditions affecting the skeletal system, bone fractures remain a major clinical concern. According to reports from the orthopedic industry, more than 50 million bone fractures are estimated to occur worldwide each year, with more than 8 million fracture-repair procedures performed annually (Goldring, M. B., & Otero, M., 2011). Bone fractures can affect individuals of all age groups and consequently represent a substantial socioeconomic burden, particularly when they occur in economically productive populations. The high incidence of bone injuries has therefore increased the demand for effective therapeutic strategies capable of restoring both the structural integrity and biological function of damaged bone. Conventional approaches for the treatment of bone defects primarily include metallic fixation devices and bone grafting. Metallic implants provide the mechanical stability required during the bone-healing process; however, conventional permanent implants generally do not actively participate in the biological processes associated with bone regeneration. Their long-term presence may also require additional surgical intervention for implant removal in certain clinical situations. Furthermore, complications associated with implant degradation, ion release, infection, and adverse host responses may limit their clinical applications (L.G. Griffith, M.A. Swartz, 2006; S. Bose, M. Roy, 2012). Bone grafting remains an important therapeutic approach and is widely considered a standard treatment for challenging bone defects. Allografts can provide structural support and biological components that contribute to bone repair; however, their use may be associated with immunological complications and limited availability of suitable donor tissue (H. J. Haugen, M. Monjo, M. Rubert, *et al.*, 2013). In contrast, autologous bone grafts possess osteogenic, osteoinductive, and osteoconductive properties, enabling them to support bone formation at the defect site. Nevertheless, harvesting autologous bone requires an additional surgical procedure, which may result in donor-site morbidity, postoperative pain, infection, and other complications. The limitations associated with conventional metallic implants and bone grafting have driven the development of alternative strategies for skeletal repair and bone regeneration. In this context, tissue engineering has emerged as a promising approach for the treatment of bone defects. Bone tissue engineering aims to develop biological or biomaterial-based systems that provide an appropriate microenvironment to support cell adhesion, proliferation, differentiation, vascularization, and subsequent formation of functional bone tissue. These strategies have the potential to promote bone regeneration while overcoming some of the limitations associated with conventional bone-repair approaches.

Hypothesis: The incorporation of silk fibroin (SF) and collagen type I into a PVA/$MgCl_2$-based scaffold is hypothesized to result in a biomimetic scaffold with suitable physicochemical and biological properties for bone tissue regeneration. The combination of these materials is expected to create a favorable microenvironment that mimics key characteristics of the native extracellular matrix (ECM), thereby promoting cell adhesion, proliferation, and subsequent tissue formation.

LITERATURE REVIEWS

Bone Tissue Engineering

Scaffolds are essential components of tissue engineering because they provide temporary structural support and a three-dimensional microenvironment for tissue regeneration (K. Kanimozhi, S. Khaleel Basha, 2016). An appropriate bone scaffold should support cell attachment, proliferation, migration, and differentiation while maintaining suitable structural characteristics. An interconnected porous architecture is particularly important for cell migration and the transport of nutrients and oxygen. Therefore, scaffold design requires an appropriate balance between structural, mechanical, and biological properties. The extracellular matrix (ECM) is a three-dimensional network that provides structural support and biochemical signals regulating cellular behavior (G. Chang et al., 2007). It contains various macromolecules, including collagen, laminin, fibronectin, glycosaminoglycans, and growth factors, which contribute to cellular adhesion, proliferation, migration, and differentiation (H.Y. Wang, Y.Q. Zhang, 2013; F. Han et al., 2014). These characteristics have motivated the development of biomimetic scaffolds designed to reproduce key structural and biological features of the native ECM. Various biomaterials, including collagen, hydroxyapatite, gelatin, and silk fibroin (SF), have therefore been investigated for bone tissue regeneration.

Silk Fibroin as a Biomaterial for Bone Tissue Engineering

Silk fibroin (SF) is a naturally derived structural protein obtained primarily from Bombyx mori. It consists predominantly of glycine, alanine, and serine, which contribute to its characteristic molecular structure and physicochemical properties (J. Melke, S. Midha, et al., 2016). SF can adopt different secondary structures, including random-coil, α-helix, and β-sheet configurations, which influence its crystallinity, mechanical properties, stability, degradation behavior, and biological performance (L-P. Yan, et al., 2012). These characteristics, together with its biocompatibility and structural stability, make SF an attractive biomaterial for tissue engineering. SF can be processed into various architectures, including fibers, films, membranes, and three-dimensional porous scaffolds. In bone tissue engineering, SF is frequently combined with other biomaterials to improve the structural and biological characteristics of composite scaffolds (T. Schuman, et al., 2004). Such composites may provide a suitable microenvironment for cellular attachment, proliferation, and differentiation, supporting their application in bone tissue regeneration.

Collagen as a Biomaterial for Bone Tissue Engineering

Collagen is a major structural component of the ECM and provides both structural support and biochemical cues for cellular interactions. Its characteristic triple-helical structure is formed by three polypeptide chains rich in glycine, proline, and hydroxyproline. In bone tissue, collagen provides an organic framework for the deposition and organization of calcium phosphate minerals, contributing to the structural integrity and mechanical properties of bone (W.S. Lyoo, W.S. Ha, 1996). Owing to its biocompatibility, hydrophilicity, processability, and ability to support cell interactions, collagen has been widely investigated as a biomaterial for bone tissue engineering.

Polyvinyl Alcohol (PVA) in Bone Tissue Engineering

Polyvinyl alcohol (PVA) is a synthetic hydrophilic polymer widely investigated for biomedical applications, including surface coatings, drug delivery systems, wound dressings, and tissue-engineering scaffolds (N.A. Peppas, J.E. Scott, 1992). Its favorable biocompatibility, low toxicity, and ability to form hydrogels with tunable physical properties have contributed to its use in biomaterial development. PVA hydrogels can be physically crosslinked using methods such as repeated freeze–thaw cycles, producing materials with water absorption, elasticity, and structural stability suitable for biomedical applications.

Magnesium Ions (Mg^{2+}) in Bone Tissue Engineering

Magnesium ions (Mg^{2+}) have attracted interest in bone tissue engineering because of their potential effects on osteoblast-related cellular responses. Previous studies have reported that Mg^{2+}-containing surfaces and apatite-based materials can enhance osteoblast adhesion and cell–material interactions. These findings suggest that incorporating Mg^{2+} into biomaterial scaffolds may provide additional biological cues that support cellular responses and contribute to the development of materials for bone regeneration.

Present Study

Based on these considerations, the present study developed a composite scaffold consisting of silk fibroin (SF), collagen type I, and polyvinyl alcohol (PVA) modified with magnesium ions (Mg^{2+}). SF was used as the base scaffold material, while collagen type I and PVA were incorporated to form the composite matrix. The SF scaffolds coated with collagen type I/PVA were treated with $MgCl_2$ at concentrations of 0, 0.5, 1, 2.5, and 5 mM to investigate the effects of $MgCl_2$ concentration. The developed scaffolds were characterized by scanning electron microscopy (SEM) and Fourier-transform infrared (FT-IR) spectroscopy to evaluate their morphological and chemical characteristics. Their biological response was further assessed using osteoblasts and the PrestoBlue assay. The study therefore aimed to investigate the effects of $MgCl_2$ concentration on the morphology, chemical characteristics, and biological response of SF/collagen type I/PVA scaffolds and to determine a suitable $MgCl_2$ concentration for further development of biomimetic scaffolds for bone tissue regeneration. From the literature review, the conceptual framework can be drawn as shown in Figure 1.

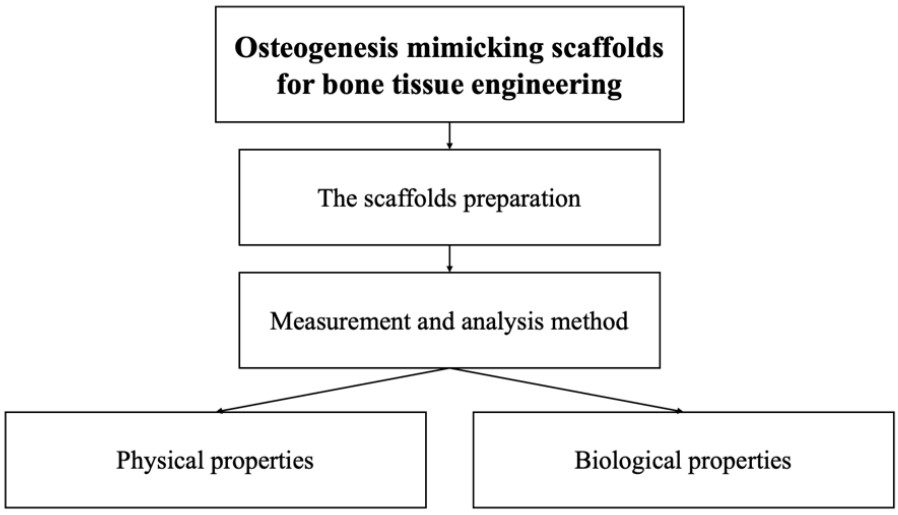


Figure 1 Conceptual Framework

RESEARCH METHODOLOGY

Preparation of Silk Fibroin Solution

Silk fibroin (SF) solution was prepared from silkworm cocoons. The cocoons were cut into small pieces and degummed by boiling in 0.02 M sodium carbonate (Na_2CO_3) solution at 90°C for 20 min. The degummed silk fibers were thoroughly rinsed with distilled water to remove residual sericin and subsequently dried in a hot-air oven at 60°C for 24 h. The dried silk fibers were then dissolved in 9.3 M lithium bromide (LiBr) solution at 70°C for 3–4 h. The resulting SF solution was transferred into a dialysis membrane and dialyzed against distilled water for 3

days, with the distilled water replaced every 6 h. After dialysis, the solution was centrifuged at 9,000 rpm at 4°C for 20 min. The purified SF solution was collected and stored at 4°C until further use.

Fabrication of Three-Dimensional Porous Silk Fibroin Scaffolds

Three-dimensional (3D) porous silk fibroin (SF) scaffolds were fabricated using a freeze-drying technique. The SF solution was dispensed into 96-well plates and frozen at −20°C for 24 h. The frozen samples were subsequently freeze-dried for 24 h to form a porous structure. The resulting porous SF scaffolds were immersed in 80% (v/v) methanol for 30 min to induce structural stabilization. Following methanol treatment, the scaffolds were subjected to a second freeze-drying process.

Collagen Type I/PVA Coating and Magnesium Chloride Treatment

The 3D porous SF scaffolds were coated with a solution containing 2% (w/v) collagen type I and 9% (w/v) polyvinyl alcohol (PVA) at a volume ratio of 12:13. The resulting collagen type I/PVA-coated SF scaffolds were subsequently treated with different concentrations of magnesium chloride ($MgCl_2$) to investigate the effect of magnesium incorporation. Five $MgCl_2$ concentrations were investigated: 0, 0.5, 1, 2.5, and 5 mM in Table 1.

Groups	Detail
A	silk fibroin film and collagen 1 + PVA
B	silk fibroin film and collagen 1 + PVA treated with 0.5 mM $MgCl_2$
C	silk fibroin film and collagen 1 + PVA treated with 1 mM $MgCl_2$
D	silk fibroin film and collagen 1 + PVA treated with 2.5 mM $MgCl_2$
E	silk fibroin film and collagen 1 + PVA treated with 5 mM $MgCl_2$

Table 1 Preparation of 3D silk fibroin scaffolds and collagen 1 + PVA treated with $MgCl_2$ will be prepared in 5 groups.

RESEARCH RESULTS

Fourier Transform Infrared (FT-IR) Spectroscopy

The molecular characteristics of the scaffolds in each experimental group were evaluated using Fourier transform infrared (FT-IR) spectroscopy with an EQUINOX 55 FT-IR spectrophotometer (Bruker Optics, Germany). The infrared spectra were recorded over a wavenumber range of 4,000–400 cm^{-1} to characterize the functional groups and chemical interactions present within the scaffold samples.

The molecular characteristics of the coated scaffolds were investigated using FT-IR spectroscopy, and the corresponding spectra are presented in Figure 2. The spectra of the control and $MgCl_2$-containing scaffolds at concentrations of 0.5, 1, 2.5, and 5 mM were compared to identify the characteristic functional groups of the scaffold components. The characteristic absorption bands of PVA, collagen type I, and silk fibroin were identified in the FT-IR spectra. The broad absorption band observed at approximately 3,500 cm^{-1} was assigned to the hydroxyl (O–H) groups of PVA. Collagen type I exhibited characteristic absorption bands at approximately 3,400 and 2,950 cm^{-1}, corresponding to amide A and amide B, respectively. The characteristic absorption bands of silk fibroin were observed at approximately 1,650, 1,550, and 1,220 cm^{-1}, corresponding to amide I, amide II, and amide III, respectively. For the experimental groups, the O–H absorption bands were observed at

approximately 3,443, 3,422, 3,450, 3,449, and 3,445 cm^{-1} for the control, 0.5, 1, 2.5, and 5 mM $MgCl_2$ groups, respectively. The amide I bands of the 0.5, 1, 2.5, and 5 mM $MgCl_2$ groups were detected at approximately 1,633, 1,633, 1,637, and 1,629 cm^{-1}, respectively. The corresponding amide II bands appeared at approximately 1,515, 1,538, 1,520, and 1,525 cm^{-1}, respectively. The amide III bands were detected at approximately 1,238, 1,238, 1,239, and 1,331 cm^{-1} for the 0.5, 1, 2.5, and 5 mM $MgCl_2$ groups, respectively. The amide A band of collagen type I overlapped with the O–H absorption band of PVA in all scaffold groups. The amide B bands were observed at approximately 2,923, 2,938, 2,924, and 2,936 cm^{-1} for the 0.5, 1, 2.5, and 5 mM $MgCl_2$ groups, respectively.

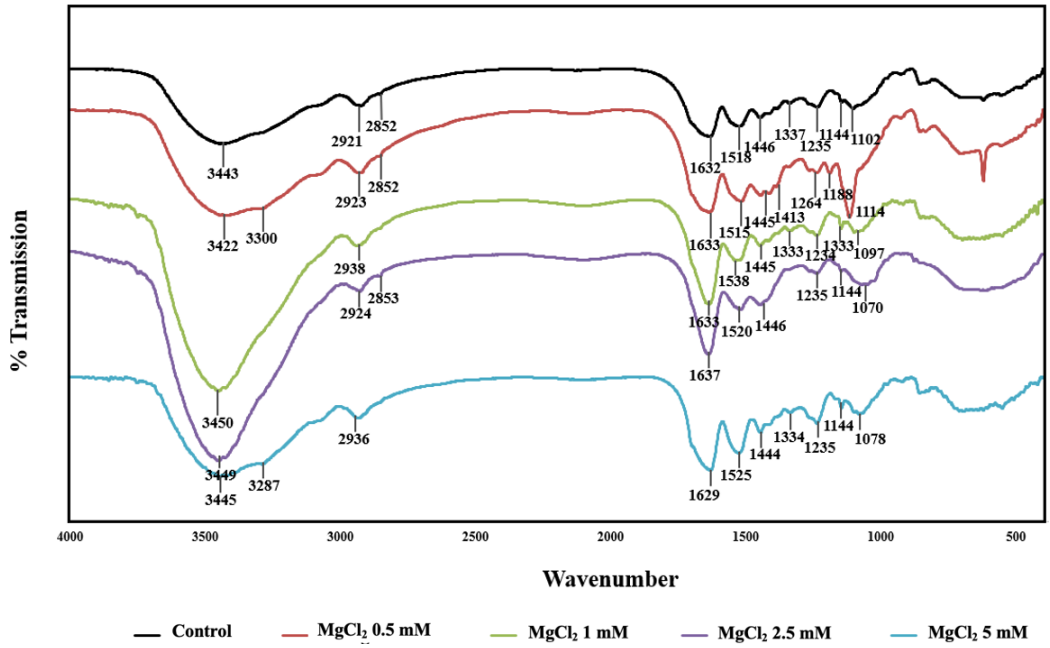


Figure 2 FT-IR spectrum of scaffold with different $MgCl_2$

Scanning Electron Microscopy (SEM) Analysis

The surface morphology of the scaffolds was examined using a scanning electron microscope (SEM; Quanta 400, FEI, Czech Republic). Prior to SEM observation, the scaffold samples were coated with a thin layer of gold using a sputter coater to improve surface conductivity and facilitate microscopic imaging.

The surface morphology of the scaffolds is presented in Figure 3. The control scaffold exhibited a relatively smooth surface, with several fibrils partially covered by a thin film. In contrast, the $MgCl_2$-containing scaffolds exhibited more pronounced fibrillar structures and fibrillar networks. The 0.5, 1, 2.5, and 5 mM $MgCl_2$ groups showed more prominent fibrillar structures compared with the control group. At lower $MgCl_2$ concentrations (0.5 and 1 mM), the fibrils appeared interconnected and were partially covered by a thin film. In contrast, the scaffolds containing higher $MgCl_2$ concentrations (2.5 and 5 mM) exhibited more distinct fibrillar structures with less apparent interconnection and without extensive film coverage. Among all experimental groups, the 5 mM $MgCl_2$ scaffold exhibited the most uniform and well-organized fibrillar network. The pore morphology also varied among the $MgCl_2$-treated scaffolds (Figure 3). The 0.5, 1, and 2.5 mM $MgCl_2$ scaffolds exhibited clearly defined porous structures with distinct pore boundaries, and the pore walls were covered by fibrillar networks. In contrast, the 5 mM $MgCl_2$ scaffold showed less apparent pore formation and a denser, highly organized fibrillar network.

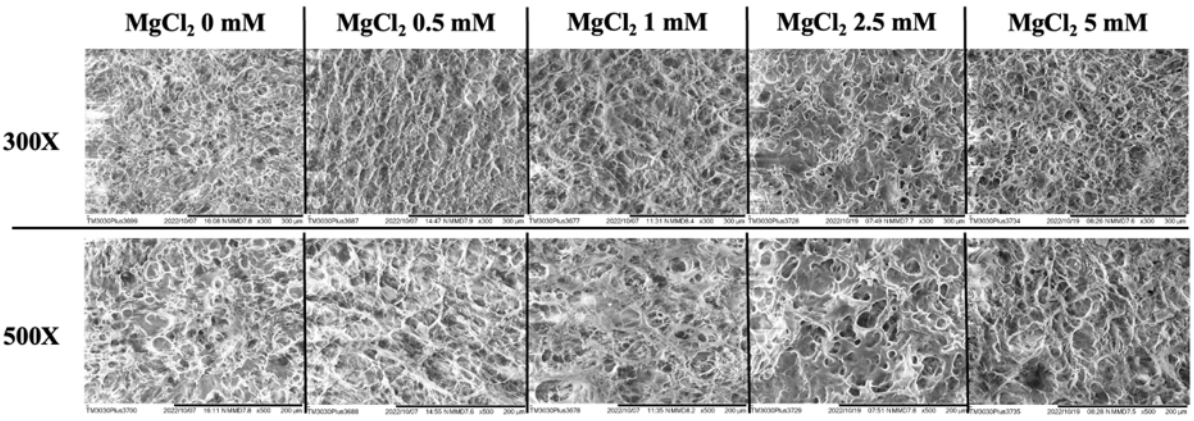


Figure 3 Surface morphology of scaffold with different $MgCl_2$

Cell Proliferation Assay (PrestoBlue™) on Days 1, 3, 5, and 7

MC3T3-E1 osteoblast cells were used in this study. The cells were cultured in α-MEM (Alpha Minimum Essential Medium) supplemented with 10% fetal bovine serum (FBS) and 1% penicillin–streptomycin. The cells were seeded in 48-well plates at a density of approximately 10,000 cells per well and maintained under appropriate culture conditions until further experiments. Cell proliferation was evaluated using the PrestoBlue™ Cell Viability Assay on days 1, 3, 5, and 7 of culture. MC3T3-E1 osteoblast cells were seeded onto the scaffolds in each experimental group and cultured under appropriate conditions. At each designated time point, the scaffolds were gently rinsed with phosphate-buffered saline (PBS) to remove residual culture medium. Subsequently, 10% (v/v) PrestoBlue™ reagent diluted in complete culture medium was added to each sample. The samples were incubated at 37°C for 1 h to allow the resazurin-based reagent to react with metabolically active cells. The resulting fluorescence was measured at an emission wavelength of 600 nm. The fluorescence intensity was used as an indicator of cellular metabolic activity and cell proliferation.

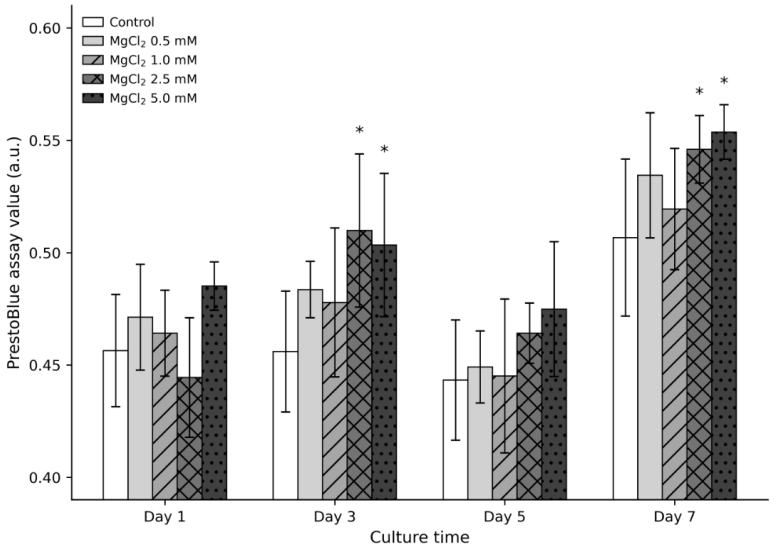


Figure 4 Cell proliferation of scaffolds with different MgCl2 at days 1, 3, 5, and 7

The proliferation of MC3T3-E1 osteoblast cells cultured on the developed scaffolds was evaluated using the PrestoBlue™ assay on days 1, 3, 5, and 7. The results demonstrated variations in cell proliferation depending on the $MgCl_2$ concentration and culture period

(Figure 4). On day 1, the PrestoBlue™ assay values ranged from 0.444 to 0.485. No significant differences were observed between any of the $MgCl_2$-treated groups and the control group ($P > 0.05$). On day 3, the 2.5 and 5 mM $MgCl_2$ groups exhibited significantly higher cell proliferation than the control group, with P values of 0.005 and 0.016, respectively. In contrast, the 0.5 and 1.0 mM $MgCl_2$ groups showed no significant differences compared with the control group ($P > 0.05$). On day 5, no significant differences were observed between any of the $MgCl_2$-treated groups and the control group ($P > 0.05$). By day 7, cell proliferation increased across all scaffold groups compared with the earlier culture periods. The highest PrestoBlue™ assay value was observed in the 5 mM $MgCl_2$ group (0.554 ± 0.012), followed by the 2.5 mM $MgCl_2$ group (0.546 ± 0.015). Both groups exhibited significantly higher cell proliferation than the control group, with P values of 0.005 and 0.021, respectively. In contrast, the 0.5 and 1.0 mM $MgCl_2$ groups did not differ significantly from the control group at day 7 ($P > 0.05$). Overall, $MgCl_2$ incorporation, particularly at concentrations of 2.5 and 5 mM, was associated with enhanced osteoblast proliferation at specific culture periods. Among the tested conditions, the 5 mM $MgCl_2$ scaffold exhibited the highest cell proliferation at day 7.

DISCUSSION

The present study investigated the effects of different $MgCl_2$ concentrations on the physicochemical characteristics and biological performance of SF/collagen type I/PVA scaffolds. The effects of $MgCl_2$ incorporation were evaluated based on FT-IR characteristics, surface morphology, and osteoblast responses. Overall, $MgCl_2$ concentration influenced the molecular environment and surface morphology of the scaffolds, while the 2.5 and 5 mM groups showed higher osteoblast metabolic activity at specific culture periods. The FT-IR spectra showed the characteristic absorption bands of PVA, collagen type I, and SF in all scaffold groups. Slight shifts in the O–H absorption band were observed among the different $MgCl_2$ concentrations, suggesting changes in the molecular environment of hydroxyl-containing groups within the scaffold. Since PVA contains abundant hydroxyl groups, these changes may be related to variations in hydrogen-bonding interactions within the polymer–protein matrix. Changes were also observed in the amide I, II, and III regions, which are associated with the protein components of the scaffold. These spectral variations suggest that $MgCl_2$ treatment affected the molecular environment of the scaffold components. However, FT-IR peak shifts alone cannot confirm the formation of specific chemical bonds between Mg^{2+} and the scaffold components. The SEM results demonstrated that $MgCl_2$ concentration affected the surface morphology and fibrillar organization of the scaffolds. The $MgCl_2$-treated scaffolds showed more prominent fibrillar structures than the control. At 0.5 and 1 mM $MgCl_2$, the fibrils appeared interconnected and partially covered by a thin film, whereas the 2.5 and 5 mM groups showed more distinct fibrils with less apparent interconnection and reduced film coverage. The 5 mM scaffold exhibited the most uniform and well-organized fibrillar network. Differences in pore morphology were also observed, with the 0.5, 1, and 2.5 mM groups showing more clearly defined pores, whereas the 5 mM group exhibited less apparent pore formation and a denser fibrillar structure. These differences may reflect changes in the organization or distribution of SF, collagen type I, and PVA within the scaffold matrix. The biological response of the scaffolds was evaluated using MC3T3-E1 osteoblasts and the PrestoBlue™ assay. No significant differences were observed between the $MgCl_2$-treated groups and the control on day 1. On day 3, the 2.5 and 5 mM groups showed significantly higher cellular metabolic activity than the control. Although no significant differences were observed among the groups on day 5, the 2.5 and 5 mM groups again showed significantly higher responses on day 7. The 5 mM group exhibited the highest PrestoBlue™ value at day 7 (0.554 ± 0.012), followed by the 2.5 mM group (0.546 ± 0.015).

The higher cellular responses observed in the 2.5 and 5 mM groups may be associated with the effects of $MgCl_2$ modification and the resulting scaffold characteristics. Magnesium ions have been reported to influence osteoblast-related cellular responses and cell–material interactions. In the present study, higher $MgCl_2$ concentrations were associated with more distinct fibrillar structures, while the 5 mM group showed the most uniform fibrillar organization and the highest PrestoBlue™ response at day 7. This correspondence suggests that the physicochemical characteristics of the scaffold may contribute to its biological response. Nevertheless, the present findings do not establish a direct causal relationship between the FT-IR changes, fibrillar morphology, and osteoblast proliferation. FT-IR, SEM, and PrestoBlue™ provide complementary information regarding the molecular characteristics, morphology, and cellular metabolic activity of the scaffolds, respectively. Overall, $MgCl_2$ concentration affected the physicochemical characteristics and biological responses of the SF/collagen type I/PVA scaffolds. The 5 mM $MgCl_2$ scaffold exhibited the most uniform fibrillar network and the highest osteoblast metabolic activity at day 7 under the conditions tested. Therefore, 5 mM $MgCl_2$ represents a condition worthy of further investigation for the development of biomimetic scaffolds for bone tissue engineering.

CONCLUSION

In conclusion, $MgCl_2$ modification influenced the molecular characteristics, surface morphology, and osteoblast proliferation of SF/collagen type I/PVA scaffolds. FT-IR analysis demonstrated changes in the molecular environment of hydroxyl and amide-containing groups following $MgCl_2$ treatment, while SEM revealed concentration-dependent differences in fibrillar organization and pore morphology. The biological evaluation demonstrated that the 2.5 and 5 mM $MgCl_2$ groups exhibited significantly higher osteoblast proliferation than the control group at days 3 and 7. Among all experimental groups, the 5 mM $MgCl_2$ scaffold exhibited the most uniform and well-organized fibrillar network and the highest osteoblast proliferation at day 7. Therefore, 5 mM $MgCl_2$ was identified as the most promising concentration among those investigated in this study. The developed SF/collagen type I/PVA scaffold modified with 5 mM $MgCl_2$ shows potential for further development as a biomaterial for bone tissue engineering. Further studies evaluating additional biological responses, mechanical properties, degradation behavior, and in vivo performance are recommended to further establish its suitability for bone regeneration applications.

REFERENCES

Arden, N., & Nevitt, M. C. (2006). Osteoarthritis: epidemiology. *Best practice & research Clinical rheumatology*, 20(1), 3-25.

Goldring, M. B., & Otero, M. (2011). Inflammation in osteoarthritis. *Current opinion in rheumatology*, 23(5), 471.

L.G. Griffith, M.A. Swartz, Capturing complex 3D tissue physiology in vitro. *Nat Rev Mol Cell Biol*. 7 (2006) 211-24.

S. Bose, M. Roy, A. Bandyopadhyay, Recent advances in bone tissue engineering scaffolds, *Trends in Biotechnology*. 30 (2012) 546-556.

H. J. Haugen, M. Monjo, M. Rubert, et al. Porous ceramic titanium dioxide scaffolds promote bone formation in rabbit peri-implant cortical defect model, *Acta Biomaterialia*. 9 (2013) 5390–5399.

K. Kanimozhi, S. Khaleel Basha, V. Sugantha Kumari. Processing and characterization of chitosan/PVA and methylcellulose porous scaffolds for tissue engineering. *Materials Science and Engineering C.* 61 (2016) 484–491.

Ferreira AM, Gentile P, Chiono V, Ciardelli G. Collagen for bone tissue regeneration. *Acta Biomater*. 2012; 8(9): 3191-200.

B.Kundu, N.E. Kurland, S. Bano, C. Patrac, F.B. Engel, V.K. Yadavalli, S.C. Kundu, Silk proteins for biomedical applications: Bioengineering perspectives, *Progress in Polymer Science*. 39 (2014) 251–267.

G. Chang, H.-J. Kim, D. Kaplan, G. Vunjak-Novakovic, R.A. Kandel, Porous silk scaffolds can be used for tissue engineering annulus fibrosus. *Eur Spine J* (2007) 16:1848–1857.

H.Y. Wang, Y.Q. Zhang, Effect of regeneration of liquid silk fibroin on its structure and characterization, *Soft Matter*. 9 (2013) 138–145.

F. Han, S. Liu, X. Liu, Y. Pei, et al. Woven silk fabric-reinforced silk nanofibrous scaffolds for regenerating load-bearing soft tissues, *Acta Biomaterialia*. 10 (2014) 921–930.

J. Melke, S. Midha, S. Ghosh, K. Ito, S. Hofmann, Silk fibroin as biomaterial for bone tissue engineering, *Acta Biomaterialia*. 31 (2016) 1–16.

L-P. Yan, J. M. Oliveira, A. L. Oliveira, S. G. Caridade, J. F. Mano, R. L. Reis, Macro / microporous silk fibroin scaffolds with potential for articular cartilage and meniscus tissue engineering applications, *Acta Biomaterialia*. 8 (2012) 289–301.

T. Schuman, M. Wikstroem, M. Rigdahl, Coating of surface-modified papers with poly (vinyl alcohol). *Surface and Coatings Technology* 183(2004)96–105.

W.S. Lyoo, W.S. Ha, Structure and properties of microfibrillar poly (vinyl alcohol) fibres prepared by saponification under shearing force of poly (vinyl pivalate). *Polymer* 37(1996) 3121–3129.

N.A. Peppas, J.E. Scott, Controlled release from poly (vinyl alcohol) gels prepared by freezing-thawing processes. *Journal of Controlled Release* 18(1992) 95-100.

Data Availability Statement: The raw data supporting the conclusions of this article will be made available by the authors, without undue reservation.

Conflicts of Interest: The authors declare that the research was conducted in the absence of any commercial or financial relationships that could be construed as a potential conflict of interest.

Publisher's Note: All claims expressed in this article are solely those of the authors and do not necessarily represent those of their affiliated organizations, or those of the publisher, the editors and the reviewers. Any product that may be evaluated in this article, or claim that may be made by its manufacturer, is not guaranteed or endorsed by the publisher.



Copyright: © 2026 by the authors. This is a fully open-access article distributed under the terms of the Attribution-NonCommercial-NoDerivatives 4.0 International (CC BY-NC-ND 4.0).